

Preparation of Reinforced Anisometric Patchy Supraparticles for Self-Propulsion

H. Esra Oguztürk, Leona J. Bauer, Ioanna Mantouvalou, Birgit Kanngießer, Orlin D. Velev, and Michael Gradzielski*

The preparation of fumed silica-based anisometric supraparticles with well-defined catalytically active patches suitable for self-propulsion is presented here. These sub-millimeter-sized particles can self-propel as they contain Pt-covered magnetite (Fe_3O_4) nanoparticles, where the Pt can decompose catalytically a “fuel” like H_2O_2 and thereby propel the supraparticles. By their magnetic properties, the catalytically active nanoparticles can be concentrated in patches on the supraparticle surface. The goal is to obtain robust supraparticles with well-defined patchiness and long-time stability during self-propulsion through evaporation-induced self-assembly (EISA) on a superhydrophobic surface. The latter is a major issue as oxygen evolution can lead to the disintegration of the supraparticles. Therefore, enhanced mechanical stability is sought using a number of different additives, where the best results are obtained by incorporating polystyrene microspheres followed by heat treatment or reinforcement with microfibrillated cellulose (MFC) and sodium trisilicate (Na_2SiO_3). The detailed internal structure of the different types of particles is investigated by confocal micro-X-ray fluorescence spectroscopy (CMXRF), which allows for precisely locating the catalytic Fe_3O_4 @Pt nanoparticles within the supraparticles with a resolution in the μm range. The insights on the supraparticle structure, together with their long-time stability, allow fabricating optimized patchy supraparticles for potential applications in propulsion-enhanced catalysis.

1. Introduction

The formation of mesoscopic superstructures built from colloidal building blocks led to numerous materials advanced in the last decades, where the different colloidal building blocks allow imparting functionality to the formed supraparticles.^[1] This approach inspired the fabrication of new well-defined hierarchically structured supraparticles,^[2] which can function as smart and functional materials^[1–6] with the capability of tuning their composition and structure. They have the potential to be used for various applications like catalysis,^[7,8] thermo- or magneto-sensitive materials,^[9–11] lithography,^[12,13] microfluidics,^[14,15] photonics,^[9,16–19] or sensing.^[20,21] The size range of such supraparticles can range from some μm to mm, where the focus of our subsequently discussed work is on particles with a size of about one mm.


Techniques that are able to synthesize such colloidal assemblies include microfluidics,^[16,22,23] spray-drying,^[17,18] and other evaporation-induced self-assembly (EISA) methods.^[24,25] For the latter, superhydro-

phobic surfaces with contact angles $> 150^\circ$ allow for symmetric evaporation from the sessile droplets resulting in spherical particles, typically in the size range of many μm to mm, formed as a result of droplet templating.^[3] When the drying droplets contain colloidal particles, these colloids become assembled together. This assembly is controlled by the interaction between the colloidal particles, leading to supraparticles with an internal structure formed during the drying process. For instance, this method allows the production of highly structured 3D-colloidal assemblies in the form of supraparticles.^[26–29] Normally one would expect this approach simply to yield symmetric spherical supraparticles.^[3] However, it has been observed that, besides spherical particles, also “doughnut”-shaped particles can be prepared^[28,30] by taking advantage of the coffee-ring effect on suspension drying.^[31,32] Silica microspheres at different concentrations were employed in such studies^[28] and the hole size of the doughnut particles can be tuned by the initial colloidal concentration and it increases with decreasing concentration. As a further materials design step, one may introduce internal structuring of the colloidal building blocks. As an example in a 2008 study, colloidal suspensions with gold nanoparticles and polystyrene (PS) latex

Dr. H. E. Oguztürk, Prof. M. Gradzielski
 Stranski-Laboratorium für Physikalische und Theoretische Chemie
 Institut für Chemie
 Technische Universität Berlin
 10623 Berlin, Germany
 E-mail: michael.gradzielski@tu-berlin.de

L. J. Bauer, Dr. I. Mantouvalou,^[†] Prof. B. Kanngießer
 Institute for Optics and Atomic Physics
 Technical University of Berlin
 10623 Berlin, Germany

Prof. O. D. Velev
 Department of Chemical and Biomolecular Engineering
 North Carolina State University
 911 Partners Way, Raleigh, NC 27695-7905, USA

 The ORCID identification number(s) for the author(s) of this article can be found under <https://doi.org/10.1002/ppsc.202000328>.

© 2021 The Authors. Particle & Particle Systems Characterization published by Wiley-VCH GmbH. This is an open access article under the terms of the Creative Commons Attribution License, which permits use, distribution and reproduction in any medium, provided the original work is properly cited.

^[†]Present Address: Helmholtz Zentrum Berlin, Albert-Einstein-Str. 15, 12489 Berlin, Germany

DOI: 10.1002/ppsc.202000328

microspheres led to the formation of highly light-diffracting supraparticles of mm size.^[27] The driving force to obtain these inhomogeneities of the colloidal components is mainly the evaporation-driven flux inside the drying droplet, which transports small gold nanoparticles to the top surface of the droplet. Subsequent studies on silica nanoparticles of different sizes showed that the bigger ones had a tendency to accumulate in the center of the formed supraparticles.^[33] Such internal sub-structuring has also been used subsequently to create catalytically active supraparticles with tunable porosity by employing sacrificial PS particles, which are removed by calcination after particle assembly.^[34] The size range of supraparticles obtained by evaporation of colloidal suspensions on superhydrophobic or superamphiphobic surfaces can easily be varied from about 50 μm to mm, as for instance show for the preparation of mesoporous TiO_2 supraparticles.^[35]

To date, most supraparticles have been assembled on the basis of PS or silica as colloidal building blocks and in general, controlling the shape of supraparticles is difficult. However, in recent work, we could show that fumed silica (FS) can be an interesting building material for such supraparticles, especially as here, the addition of small amounts of NaCl allows to control the shape of the formed supraparticles. Their anisometry increases with increasing NaCl concentration in the drying suspension droplets of FS as shown by Sperling et al.^[29]

In our present research, we were interested in fabricating anisometric supraparticles containing a catalytically active patch enabling self-propulsion due to asymmetric catalytic decomposition. For this purpose, we employed FS and controlled the anisometry by the NaCl concentration in the suspension phase. The ability for self-propulsion was imparted by incorporating $\text{Fe}_3\text{O}_4@\text{Pt}$ core-shell nanoparticles within the formation process (see **Figure 1**), where the magnetic properties of the core are used to steer the $\text{Fe}_3\text{O}_4@\text{Pt}$ nanoparticles to a certain location within the supraparticles, as shown previously.^[36]

A main problem for the use of such porous FS-based self-propelling supraparticles in catalytic applications is fragility, which may lead to rapid disintegration in the solution. Accordingly, enhancing their lifetime under self-propulsion conditions, that is,

in the presence of aqueous H_2O_2 solutions, was the key question addressed within this work. The main problem arises from the fact that the production of O_2 during the catalytic decomposition of H_2O_2 is not only at the origin of self-propulsion but the O_2 can also accumulate within the pores of the supraparticles, leading to a pressure build-up that can destroy them. In order to avoid this, various approaches were employed, including hydrophobization, in order to avoid the formation of O_2 within the internal pores of the supraparticles, and the incorporation of PS, microfibrillated cellulose (MFC), and sodium silicate (Na_2SiO_3), as additional building blocks for enhancing the mechanical stability. Especially MFC is interesting here as means of strongly reinforcing the internal structure and the properties of the supraparticles as its fibrillar content introduces a strongly anisometric building block. For instance, cellulose nanofibrils have been shown to increase largely the toughness of supraparticles.^[37] In addition, MFC is biocompatible, which widens the potential application areas of the particles. MFC fibrils have diameters of 5 nm – 60 nm and lengths of several micrometers.^[38] It has been used for many areas of application not only because of its abundance in nature, but also due to its unique properties such as high surface area, high viscosity at low temperatures, and being extremely robust to pH and temperature.^[39] As shown in this work the optimized use of these properties allowed to produce long-time stable self-propelling supraparticles.

2. Preparation and Methods

2.1. Materials

The materials used for the preparation and the modifications of the particles used in this study are listed in the **Table 1** below.

2.2. Preparation of $\text{Fe}_3\text{O}_4@\text{Pt}$ Nanoparticles

As a first step, the synthesis of Fe_3O_4 nanoparticles was performed based on the procedure reported by Kang and coworkers.^[40]

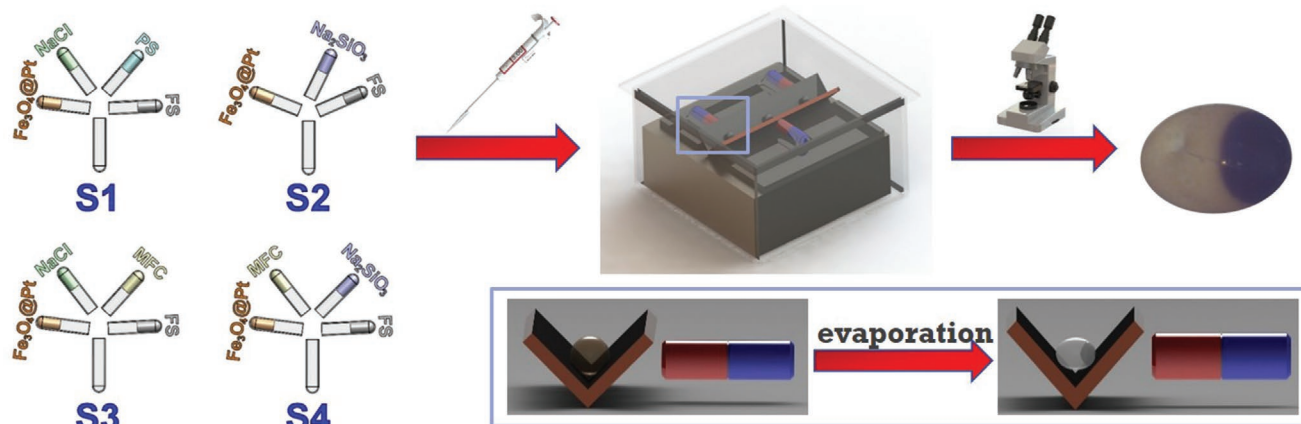


Figure 1. Scheme for the preparation of the patchy supraparticles: Four types of patchy particles having different compositions were obtained via EISA method in the presence of magnets in the set-up. (S1: FS, NaCl, PS, and $\text{Fe}_3\text{O}_4@\text{Pt}$; S2: FS, Na_2SiO_3 , and $\text{Fe}_3\text{O}_4@\text{Pt}$; S3: FS, NaCl, MFC, and $\text{Fe}_3\text{O}_4@\text{Pt}$; S4: FS, Na_2SiO_3 , MFC, and $\text{Fe}_3\text{O}_4@\text{Pt}$).

Table 1. List of all materials used in this work with supplier and specifications.

Materials	Specifications	Supplier
FS AEROSIL 90	surface area = $90 \pm 15 \text{ m}^2 \text{ g}^{-1}$	Evonik
PS-latex	$d = 0.96 \text{ }\mu\text{m}$, $\rho_{\text{solid}} = 1.05 \text{ g mL}^{-1}$ $c_{\text{solid}} = 10\% \text{ w/v}$	Bangs-Labs
NaCl	synthesis-grade, $\geq 99.9\%$	ChemSolute
Na_2SiO_3	$\geq 18\%$ Na (as Na_2O) basis, $\geq 60\%$ Si (as SiO_2) basis	Sigma-Aldrich
MFC	grade HP-55, M_w 84 000 g mol^{-1} , M_n 21 000 g mol^{-1}	Shin Etsu Chemical Co.
MiliQ water	$\geq 18 \text{ M}\Omega \text{ cm}^{-1}$	
H_2O_2	30% wt	Sigma-Aldrich
NaBH_4	$\geq 96\%$	Sigma-Aldrich
$\text{H}_2\text{PtCl}_6 \cdot 6\text{H}_2\text{O}$	$\geq 37.5\%$ Pt basis	Sigma-Aldrich
Sodium Citrate Tribasic Hydrate	ACS reagent, $\geq 99.0\%$	Sigma-Aldrich
HCl	aqueous, 37%w/w	Merck
NaOH	ACS-grade, $\geq 98\%$, pellets	Fluka
$\text{FeCl}_2 \cdot 4\text{H}_2\text{O}$	$\geq 98\%$	Sigma-Aldrich
$\text{FeCl}_3 \cdot 6\text{H}_2\text{O}$	ACS-grade, $\geq 98\%$	Sigma-Aldrich

5.2 g $\text{FeCl}_3 \cdot 6\text{H}_2\text{O}$ and 2.0 g $\text{FeCl}_2 \cdot 4\text{H}_2\text{O}$ (molar ratio: $\text{Fe(II)}/\text{Fe(III)} = 0.5$) were dissolved in 25 mL of deoxygenated water and combined with 0.85 mL of 12 M HCl added under stirring. The resultant solution was added to 250 mL of 1.5 M NaOH solution to neutralize the suspension under vigorous stirring. The appearance of an instant black precipitate was proof of Fe_3O_4 nanoparticle formation. The magnetic particles were separated easily with the help of a magnet and purified by decantation.

Subsequently, $\text{Fe}_3\text{O}_4@Pt$ formation was performed with $\text{H}_2\text{PtCl}_6 \cdot 6\text{H}_2\text{O}$ at room temperature by a conventional reduction method with NaBH_4 in the presence of sodium citrate tribasic hydrate. 114 μL $\text{H}_2\text{PtCl}_6 \cdot 6\text{H}_2\text{O}$ solution ($c = 0.1 \text{ M}$) was added to 95 mL of the previously synthesized Fe_3O_4 solution (0.02%w) dropwise within 1 min. After 2 min, 1.5 mL of ice-chilled 0.01 M NaBH_4 solution was added dropwise in 1.5 min. 1 min after NaBH_4 addition, 1 mL of 0.5 M sodium citrate solution was added at once. This solution was then stirred for 3–5 min more at 7200 rpm speed with an ultra turrax. The resultant solution was centrifuged for 15 min at 4000 rpm 3 times to remove the impurities and concentrate the solution. Afterwards, the weight percentages of the Fe and Pt in the catalyst were determined by ICP-OES [Varian ICP-OES 715 ES] measurement. Before ICP-OES, in order to dissolve Pt in Fe_3O_4 , microwave treatment of the sample was necessary in the presence

of aqua regia. The data derived from ICP-OES established that, Fe^{3+} and Pt concentrations were 11.79 and 0.69 mg L^{-1} , respectively, from which the concentration of the synthesized $\text{Fe}_3\text{O}_4@Pt$ in the sample was calculated as 0.17%wt. This solution was then used as a stock solution for the preparation of the droplets used in the formation of the supraparticles.

In order to obtain structural information about the nanoparticles formed, transmission electron microscope (TEM) images were collected with an FEI Tecnai G² 20 S-TWIN TEM. In Figure S1a,b, Supporting Information, electron micrographs of Fe_3O_4 and $\text{Fe}_3\text{O}_4@Pt$ samples are shown and in Figure S1c, Supporting Information, a SAED (Selected Area Electron Diffraction) pattern from the indicated region of the $\text{Fe}_3\text{O}_4@Pt$ sample was obtained which demonstrates the presence of Fe_3O_4 and Pt by comparison to the database of The International Centre for Diffraction Data.^[41,42] Dark-colored agglomerates in the second image (Figure S1b, Supporting Information) refer to randomly distributed Pt on the Fe_3O_4 nanoparticles. The size of the synthesized $\text{Fe}_3\text{O}_4@Pt$ particles lies in the range of 8–12 nm (see Figure S1d, Supporting Information).

2.3. Preparation of Patchy Supraparticles

First, a concentrated stock suspension of FS ($\approx 0.3 \text{ g FS}$ in 75 mL deionized water) was prepared by dispersing FS particles in deionized water and the suspension was stirred for 3 h at 1200 rpm with a magnetic stirrer at room temperature. Then, the suspensions were centrifuged (20 min at 5000 rpm) to obtain a concentrated solution (concentration $\approx 10\text{--}15\% \text{ wt/v}$), which then was diluted to 7% wt/v. The resultant solution was slightly acidic with pH 5.7 and milky looking.

For the preparation of the FS-based patchy particles (see Figure 1 for the general approach) the 7% wt/v pre-prepared FS suspensions were mixed with differently concentrated electrolyte (NaCl) solutions and a dispersion of 0.017% wt/v magnetic/catalytic nanoparticles ($\text{Fe}_3\text{O}_4@Pt$). As the long-term aim was to produce particles suited for self-propulsion, control of the final shape of the droplets is of central importance. After trials with different NaCl concentrations (5–50 mM), we decided to fix the concentration of the initial NaCl stock solution to be added to the colloidal mixture at 10 mM here, which dilutes to 2.5 mM in the final colloidal mixture to obtain nicely elliptical particles (see Figure 2). For that purpose, a 100 mM NaCl stock solution was prepared and diluted as needed. As described previously,^[29] the anisometric shape arises because, during the drying process of the droplets on a superhydrophobic surface, the FS particles accumulate on the water/air surface of the shrinking droplet. The presence of NaCl reduces the electrostatic repulsion



Figure 2. Optical micrographs of the different types of supraparticles prepared with different colloidal compositions (scale bar: 500 μm and same for all images).

between the FS particles, leading to the formation of an increasingly stronger crust on the surface of the shrinking particles. As they then have to shrink further under the constraint of a fixed surface area, anisometric supraparticles are formed. Via the concentration of NaCl one controls the extent of anisometry of the formed particles.^[29] If bent superhydrophobic surfaces are used as substrate (see Figure 1) one can control the direction of the elongation of the particles, which will be perpendicular to the V-shape of the bent surface.^[41] This then allows to form patches of magnetic particles in a well-defined manner on the surfaces of such particles, by directing them with an appropriately placed magnet.^[41]

In the further studies aimed at enhancing the mechanical stability of the supraparticles, PS, Na₂SiO₃, or MFC were added to the colloidal dispersion, which was transformed into supraparticles by evaporation. The idea here was that trisilicate could bridge between FS particles and thereby strengthen their connection, while the MFC was thought to be able to form an independent network within the supraparticles and by itself is a material much less brittle than silica and thereby should provide additional elasticity to the material. For that purpose, 10 wt% PS latex, 1.5 wt% MFC dispersions, and 0.1 M Na₂SiO₃ solution (all are initial concentrations of the additives) were added in different ratios to the colloidal mixture. However, the main material of the supraparticles always remained FS.

The volumes of FS and Pt catalyst were fixed in the procedure; while NaCl, PS, Na₂SiO₃, and MFC amounts were changed to obtain particles having different properties to be investigated. These 4 types of particles were named as: Sample 1 (S1) containing PS, Sample 1^a & Sample 1^b (S1^a and S1^b) have the same composition as S1, the only difference is the additional heat treatment and hydrophobization agent applied to S1^a and S1^b respectively after drying, Sample 2 (S2) contains Na₂SiO₃, Sample 3 (S3) MFC, and Sample 4 (S4) MFC and Na₂SiO₃. Sample 0 (S0) is the reference sample of pure FS, NaCl, and Pt catalyst to be developed further for self-propulsion purposes by the admixture of the different additives. The compositions of all final particles are given in detail in Table 2. Detailed information is given in Sections 2.2 and 2.3. The preparation of the reference sample without Pt catalyst (P0) was performed by mixing the main material FS with NaCl to end up with a particle having desired shape (anisometric). For S0, S1, S1^a, S1^b, and S3, NaCl was used as an electrolyte to give anisometry to the final particles; while in S2 and S4, Na₂SiO₃ was used instead of NaCl to benefit from both being an electrolyte for the sake of anisometry and the contributions to the mechanical properties of the particles.

Table 2. Final compositions (in dry state) of the different types of supraparticles prepared and investigated.

Samples/Components wt%	Type P0	Type S0	Type S1,S1 ^a ,S1 ^b	Type S2	Type S3	Type S4
Fumed Silica	99.17	98.47	86.33	84.37	97.09	91.12
NaCl	0.83	0.33	0.29		0.12	
Fe ₃ O ₄ @Pt		1.20	1.05	1.03	0.71	1.11
Polystyrene			12.33			
Na ₂ SiO ₃				14.60		6.38
MFC					2.08	1.47

For the formation of catalytically active supraparticles; FS, electrolyte, Fe₃O₄@Pt, and potential additive(s) for stabilization were mixed into a homogeneous dispersion by Vortex stirring in a vial. 3 μL droplets of this dispersion were then placed on a 90° bent superhydrophobic surface (see Figure 1), which was prepared as previously described.^[36] In all cases, these droplets of the initial colloidal dispersion were then let to dry, thereby yielding the final supraparticles.

In order to obtain patches made of Fe₃O₄@Pt nanoparticles, the nanoparticle suspension was pulled to a certain position of the forming supraparticles with the help of attractive magnetic forces, by fixing NdFeB cylinder magnets with Nickel coating (flux density inside: 1.37 Tesla, flux density on the surface: 0.5856 Tesla^[43]) on a chosen side of the superhydrophobic surface. With the bent superhydrophobic surfaces, one controls the direction of the supraparticles and by the relative magnet orientation the position of the catalytically active patch.

The colloidal mixture prepared with the initial components (see Table 2) has a brownish color due to the catalyst. After depositions of the droplet on the superhydrophobic surface as the time passes during drying, the droplets become lighter in color with a dark part on the side where the magnet was fixed, as the magnet was attracting the magnetic catalytic nanoparticles to one side of the supraparticles. When the droplet is completely dry, a yellowish-white elliptical particle with a well-defined “eye-like patch” was obtained. Step-wise patch formation is illustrated in Video S1, Supporting Information, with the frames selected from an animation (prepared in Autodesk Maya software^[44]).

Optical micrographs of the prepared sample types P0, S1, S2, S3, and S4 are shown in Figure 2. As clearly seen, P0 is opaque white; S1, S2, and S4 are yellowish-white with a finely localized dark patch. S3 was also expected to be a nicely patchy particle; however, due to the MFC contents, the catalyst was trapped within the bulk of the particles during evaporation. This phenomenon will be explained in detail in Section 4.2.3.

2.4. Self-Propulsion Experiments and Stability Experiments in H₂O₂ Solution

For testing of the self-propulsion properties and stability during the propulsion dynamics, the obtained patchy particles were put in a plastic petri dish (diameter of 9 cm) filled with 5% H₂O₂. Within a few seconds, wetting occurs, and platinum starts to catalyze the decomposition reaction of H₂O₂ thereby giving rise to the formation of H₂O and oxygen gas. Oxygen bubble formation on the patchy side of the particle and when the oxygen is released from the supraparticles' surfaces, they

start moving in the opposite direction due to conservation of momentum.^[45] The whole process was monitored with a digital camera (CANON EOS 5D MARK II).

3. Instrumentation Methods

3.1. Optical Microscope (OM)

Dried patchy particles were analyzed with an optical microscope (OM) for determining their anisometry (USB-cam DFK 72AUC02 connected Carl Zeiss Jenapol OM with a Planchromat LD 4x objective) at TU Berlin. IC-Capture Software was used to record the images and Fiji/Image J Software was employed for the calculation of the anisometry.^[46] For the studies conducted at North Carolina State University (NCSU), optical micrographs were taken with a BX61 Olympus microscope.

3.2. Scanning Electron Microscope (SEM)

Scanning electron micrographs of the supraparticles were taken at the TU Berlin at the ZELMI with a Hitachi S-2700 SEM, while at NCSU, a Field Emission SEM-FEI Verios 460L was employed.

3.3. Transmission Electron Microscope

TEM studies were performed at the TU Berlin ZELMI with an FEI Tecnai G2 20 S-TWIN type TEM.

3.4. Confocal Micro-X-Ray Fluorescence Spectroscopy (CMXRF)

Confocal Micro-X-Ray Fluorescence Spectroscopy (CMXRF) studies were performed at TU Berlin with a laboratory setup using a Mo microfocus X-ray tube, two polycapillary lenses, and an SDD detector.^[47] All experiments were performed with 50 kV and 600 μ A voltage and current of the tube, 30 and 40 μ m pixel size, and 5 to 15 s measuring time per pixel. For the experiments, the supraparticles were attached to a sticky carbon tape.

4. Results and Discussion

The Fe_3O_4 @Pt containing supraparticles were formed with the purpose of eventually being useful as self-propelling particles in an H_2O_2 containing aqueous solution. However, in order to be employed for such experiments, they have to be structurally long-lived and also to retain their catalytic performance. Accordingly, the mechanical stability and integrity of these supraparticles are of central importance for this planned application.

4.1. Disintegration of $\text{FS}/\text{Fe}_3\text{O}_4$ @Pt Supraparticles during Self-Propulsion

The components in the initial colloidal mixture are all hydrophilic, with the main component being FS. Accordingly, they

were fully wetted when immersed in H_2O_2 solution, including the pores of the supraparticles. However, under this condition, O_2 gas formation will also take place within the pores, and the resulting capillary pressure leads to a substantial mechanical strain within the pores. This can result in the disintegration of the supraparticles after being immersed in an H_2O_2 solution, as observed experimentally. The particles prepared with FS, NaCl, and the catalyst (S0) were observed to disintegrate completely as soon as they are put into H_2O_2 solution as expected (see Video S2, Supporting Information). This phenomenon brought up the necessity of the modification of the particles.

4.2. Modifications for Enhancing the Stability of $\text{FS}/\text{Fe}_3\text{O}_4$ @Pt Supraparticles

As just pointed out the first major problem affecting the supraparticles stability is their hydrophilicity, which allows H_2O_2 to enter, which leads to subsequent gas release within their pores, and the build-up of capillary pressure within them. The second problem is their brittleness and general fragility, as the dry silicate-based systems tend to crack and disintegrate rapidly. In order to eliminate this problem, we investigated various approaches to fabricate hybrid material supraparticles, detailed below, to prevent particle disintegration, by reducing the hydrophilicity of the supraparticles and enhancing the mechanical strength of their constitutive material.

4.2.1. Incorporation of PS Latex Particles (Type S1)

As the first type of particle composition, PS was added into the colloidal mixture in order to enhance particle stability by forming a composite silica/polymer particle. The hypothesis was that PS may act here not only as a mechanical strengthening and hydrophobization agent, but also to improve the swimming ability of the particles as PS has a lower density (1.05 g cm^{-3}) than the rest of the supraparticles material (densities of the components in the colloidal mixture of FS, Fe_3O_4 , Pt, and NaCl are: 2.2, ≈ 5.17 , 21.45, and 2.16 g cm^{-3} , respectively). For the purpose of particle modification, PS latex was added via a solution with a concentration of 10.0 wt%. A secondary function expected of PS was to effectively glue together the FS network. When very small amounts of PS (below 5 v% relative to the dry supraparticles) were present, no significant effect could be achieved with respect to enhancing stability. Therefore, higher amounts of PS (10 v% with respect to the dry supraparticles) were added to optimize the procedure. However, in that case, particles became brittle and were breaking into several pieces during the drying process.

The particles modified with PS within the first few seconds after being placed into the 5 wt% H_2O_2 solution, exhibited typically mechanical disintegration, as shown in the images given in **Figure 3** (which were taken from the videos (Video S3 & Video S4, Supporting Information)) of the self-propulsion experiments. Each row exemplifies the disintegration of a single particle within the experiment. In addition, the wetting of the supraparticles increases their probability of sinking into the solution and not swimming on its surface, as desired for

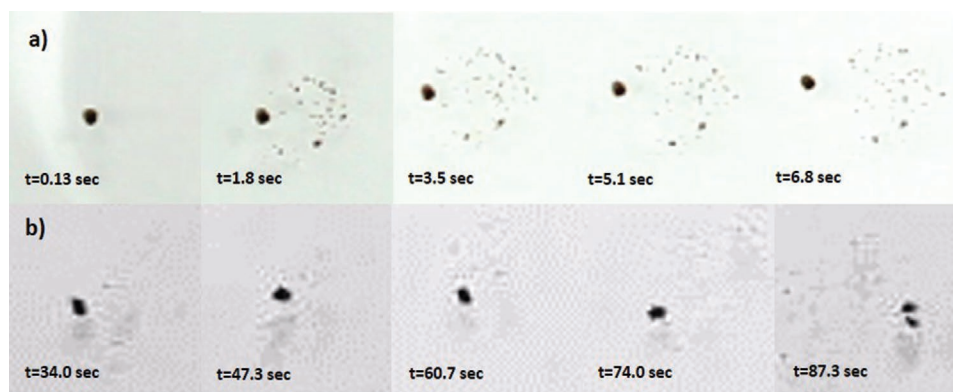


Figure 3. Examples of disintegration of two S1 type supraparticles (PS modification) (S1-a & S1-b). (Frames were picked from the recorded videos of self-propulsion experiments, $t = 0$ refers to the time at which the particle is placed on the aqueous H_2O_2 solution; displayed frame area: $8.2 \text{ cm} \times 8.2 \text{ cm}$). Particle disintegration starts when the particle contacts the H_2O_2 solution (wetting). This phenomenon causes some particles to begin disintegrating within a few seconds like in case (a), or after tens of seconds like in case (b) above. In these images one sees also the formation of O_2 bubbles, taking place on one side of the supraparticles.

such particles. All this constitutes a serious problem for making reliable self-propelling systems and accordingly, we wanted to improve the stability of such particles in H_2O_2 solution.

The degree of disintegration of the particles was evaluated via the decrease of their projected area in the images like the ones shown in Figure 3. In Figure 4, the decrease of this area (relative to the initially present area, $t = 0$) is plotted as a function of time for type S1-a and S1-b particles. As seen from the graphs, the particles lose 40–50% of their projected area within about 4–5 s. For some particles, this time may be delayed by a certain time that is required for wetting to occur. After losing around 40–50%, the particles were stable and further disintegration was not observed. Apparently, without additional treatment, the supraparticles are disintegrating largely in a few seconds. Therefore, in order to render them suitable for self-propulsion one has to enhance their stability in solution.

Supraparticles' Heat Treatment (Type S1^a): In order to prevent the disintegration of the particles, we decided to combine PS addition with subsequent heating. As PS has a glass transition temperature of $\approx 100 \text{ }^\circ\text{C}$, heating above $100 \text{ }^\circ\text{C}$ allows for softening/melting of the PS lattices, which then can form a much more homogeneous and interconnected matrix with the FS, as seen in Figure 5. Accordingly, 5 v% of PS from 10 wt/v% stock

(12.33 wt% in dry particle) were added to the colloidal mixture and as soon as particles started to become dry, they were placed in an oven for few (3–4) hours at around $100\text{--}120 \text{ }^\circ\text{C}$. Figure 5 indicates that the PS spheres appear to be randomly distributed in the unheated particle (left), while in the study of Zellmer and coworkers^[33] larger particles were observed to accumulate in the particle center. However, in the sintered particle (right) the PS lattices have disappeared, and a relatively homogeneous composite material is formed. Accordingly, one may expect that the PS now works as a binding agent for the FS and makes the particle mechanically more durable.

In addition to PS's melting, heat treatment is contributing to improved stability via hydrophobization of the particles, as the number of free Si-OH groups is reduced by a condensation reaction in which H_2O becomes eliminated,^[48] and more hydrophobic Si-O-Si bridges are formed instead. This reaction in general leads also to more compact particles and reduces their porosity. The main control parameters are temperature and time of heating.

For the heat treatment, the dried supraparticles were kept in an oven at around $110\text{--}120 \text{ }^\circ\text{C}$ for 4–20 h. It was observed that heating for 4 h was not enough for sufficient hydrophobization to prevent disintegration; however, heating for longer times,

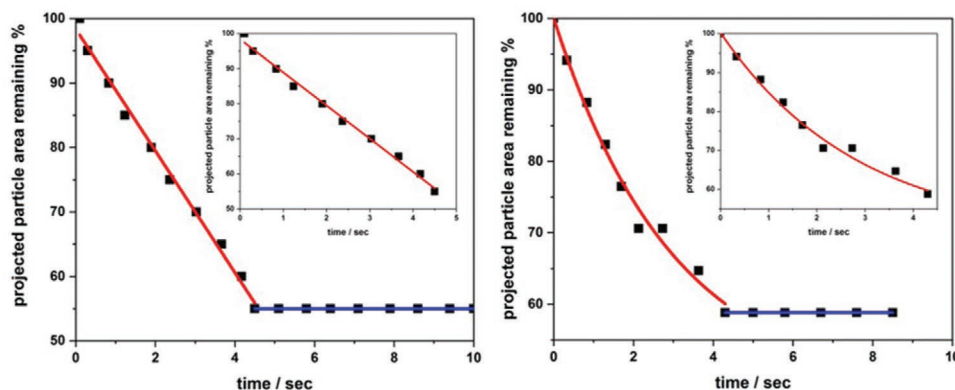


Figure 4. Disintegration profiles of two S1 type supraparticles (Left: S1-a & Right: S1-b from Figure 3) with time ($t = 0$ refers to the time at which wetting occurs; lines are guides to the eye). Particles become stable in size after a few seconds.

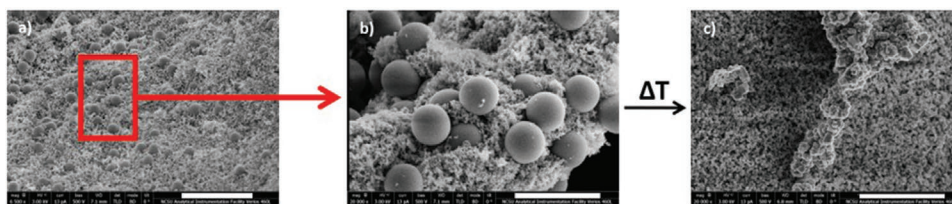


Figure 5. SEM images for the sintering process of PS under heat treatment. a,b) Before heat treatment, and c) after heating above the glass transition temperature (T_g). Melting of the PS latex is observed clearly in the image on the right after heat treatment. (Scale bars: (a) 5 μm ; (b,c) 2 μm)

that is, 16–20 h, resulted in over-hydrophobization and inactivation of the catalytic activity (see Video S5, Supporting Information). The particles heated for 8 h were found as both stable and reactive; therefore, moderate heating conditions were defined as 8 h for these particles.

Supraparticles' Treatment with Hydrophobization Agent (Type S1^b): Another approach to hydrophobize the particles was conducted by using trichloro methyl silane ($\text{CH}_3\text{Cl}_2\text{Si}$) as a functionalization agent. The process is based on chemical vapor deposition (CVD) of trichloromethyl silane on the particle. Due to its high reactivity, $\text{CH}_3\text{Cl}_2\text{Si}$ reacts with the free Si-OH groups on the surface of the supraparticles, which are responsible for their otherwise intrinsic hydrophilicity. CVD was accomplished by simply putting the particle and 5–10 μL of $\text{CH}_3\text{Cl}_2\text{Si}$ in separate petri dishes close together (2 cm distance) in a closed chamber for a few seconds.

However, even though the time for CVD with $\text{CH}_3\text{Cl}_2\text{Si}$ was kept very short (≈ 10 s), the reaction was proceeding too far. This means that wetting of the supraparticles was prevented, but at the same time apparently, the catalytically active sites were covered and inactivated as well, which resulted in failure of self-propulsion of these modified supraparticles as in the previous case (4.2.2) caused by over-heating.

In contrast, when CVD was performed for shorter times (3–5 s), partial hydrophobization occurred which could not prevent particle disintegration during self-propulsion. In general, it can be concluded that this method is not suitable as it was not possible to choose an appropriate contacting time that allowed to have good control over the hydrophobization process.

4.2.2. Incorporation of Na_2SiO_3 (Type S2)

Sodium silicate, or “water glass”, has been widely used in various materials as an adhesive agent to keep silica-based components together.^[49] Accordingly, we also used Na_2SiO_3 in order to enhance the mechanical stability of our FS-based supraparticles. It was observed that below concentrations of 0.1 M in the initial colloidal mixture, Na_2SiO_3 does not have a significant effect on the anisometry of the dried particles, however above 0.5 M the particle shapes become irregular. Therefore, for incorporation of Na_2SiO_3 , droplets containing 0.2 M Na_2SiO_3 solutions were added to the mixture and 3 μL droplets of the mixture were templated on superhydrophobic surfaces to obtain patchy particles. Light microscopy images of the thus obtained anisometric supraparticles are shown in **Figure 6**. Na_2SiO_3 containing particles did not disintegrate during self-propulsion experiments

in H_2O_2 solution (see Figure 13); therefore, by using Na_2SiO_3 , one can provide completely stable particles for self-propulsion purposes.

4.2.3. Incorporation of MFC into Supraparticles (Type S3)

MFC was employed as a further modifying agent, which may help to improve the structural integrity and by its lower density (compared to the core components) also increase the buoyancy of the formed particles. MFC is also interesting due to its highly porous internal structure and its unique properties (high surface area, high aspect ratio, high viscosity at low temperatures, being extremely robust to pH and temperature, ability to form strong microfiber films with excellent barrier properties, etc.^[39]). Therefore, we considered it to be an interesting additive that might aid in the formation of supraparticles with well-defined anisometry, improve their mechanical properties, and introduce additional functionality (for instance higher meso- and microporosity) to the systems.

In our experiments, we started with high concentrations of MFC (i.e., 10 wt% relative to dry particle and higher). However, at such higher concentrations, the transport of the catalytic nanoparticles to the magnet is hindered, presumably due to the crowded internal media. This phenomenon causes irregular shape and inhomogeneous dispersion of the catalyst inside the final particle as seen in **Figures 2** and **7**.

To obtain regularly shaped particles with well-defined patches (with such irregularly shaped particles as depicted in Figure 7 one would not expect to obtain a well-defined behavior in self-propulsion), we decreased the MFC amount to 1.5 wt/v (1.47 wt% of the final dry supraparticle) and observed that MFC brings its characteristic fibrillated structure to the system without causing irregularities in the shape as shown in **Figure 8**. To gain a better insight, the middle part of the particle

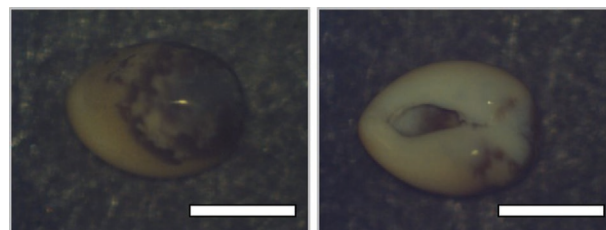


Figure 6. 4x microscopy images of a Na_2SiO_3 associated FS-based particle (front and back side of the same particle, scale bar: 0.5 mm) (S2, for composition, see Table 2). Clear separation of the patch was achieved for Na_2SiO_3 containing FS-based particles.

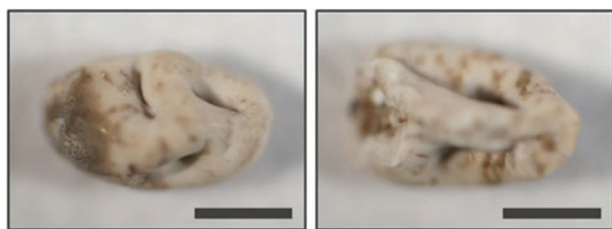


Figure 7. Microscope images of two different MFC-associated (S3) FS-based particles (scale bars: 0.5 mm; MFC content in the final supraparticle is 2.08 wt%). For such high amounts of MFC, both internal and surface inhomogeneities are occurring.

was 5x magnified and is shown on the right side. MFC provides a homogeneously distributed network structure to the particles' internal alignment, with a relatively smoother surface as evaporation occurs from outside to inside. However, the concentration must be adjusted carefully.

4.2.4. Incorporation of MFC and Na_2SiO_3 (Type S4)

In order to obtain even more regularly shaped MFC modified particles, not only the MFC amount was decreased (from 2.08 to 1.47 wt% in the final particle) but also Na_2SiO_3 was added (S4). Optical microscopy images of such an S4 particle are shown in **Figure 9**. When compared to the particles with a higher MFC amount (2.08 wt%, **Figure 7**), it is observed that S4 particles (1.47 wt%) obviously have more regular shapes with a more homogeneously looking distribution of the catalyst located on one side.

4.3. Visualization of the Internal Structure of the Particles

For a thorough understanding of the supraparticles' properties, a detailed characterization of their structure is required. Accordingly, all particles were analyzed by optical microscopy to determine their shape and their average anisometry (see **Table 3**). However, optical microscopy images only allow to image the surface, that is, the overall shape. They do not give detailed information about the internal structure of the supraparticles, especially with respect to the distribution of the catalytically active $\text{Fe}_3\text{O}_4@\text{Pt}$ nanoparticles, which is important for their potential use in self-propulsion, as the detailed form and position of the catalytically active patch should largely affect the propulsion process. It is clearly seen from the optical

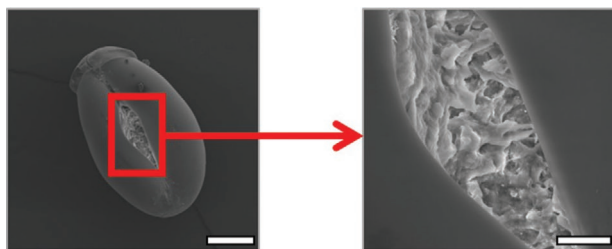


Figure 8. SEM image of an MFC-containing FS-based particle (S4; for the composition see **Table 2**) (Scale bar: left: 300 and right: 60 μm).

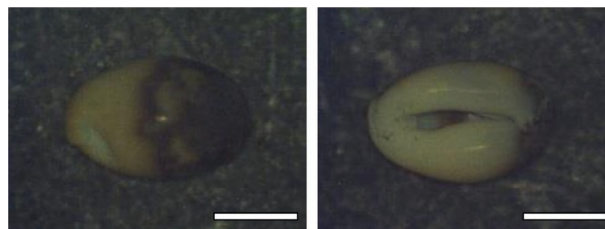


Figure 9. Microscope images of MFC & Na_2SiO_3 -associated FS based particles (S4); scale bars: 0.5 mm. The joint addition of MFC & Na_2SiO_3 ensures regular shapes and homogeneous distribution of the ingredients.

microscopy images (see **Figure 2**) that the particles were having a smooth elliptical shape with a dark patch on one side. Here, a few interesting yet still open questions are how deep this catalytically active patch goes into the supraparticle, if the shape of the patch depends on the composition of the particles, and what is the distribution of the catalytically active nanoparticles within the supraparticles.

A potential technique to address that question is SEM, but for its application, one would have to cut the particles which could introduce artifacts in observing their internal structure by SEM. Alternatively, CMXRF is a more adapted and much less invasive investigation tool. This method allows the elemental imaging of specimen in 3D, in our case with a resolution of roughly 30 μm .^[50–52] Due to the low density of the particles the internal localization of Fe and Pt can be performed without the need for sectioning. Multiple experiments on all classes of supraparticles were performed by means of CMXRF with the supraparticles being attached to a carbon tape. In **Figure 10**, the results of a measurement of a supraparticle prepared with Na_2SiO_3 (type S2) in absence of an applied magnetic field during the formation process are presented as an example (see **Figures S3–S6**, Supporting Information) for results of measurements on the other classes of particles).

Visualized are virtual slices through the particle with a 30 μm distance between the slices and 30 μm pixel size. For virtual slices along a different axis see **Figure S5**, Supporting Information. In the case of the particle from **Figure 10**, the overall shape is elliptical with a round part on the top, a hole in the middle, and a crescent-shaped part on the bottom. Fe and Pt are distributed approximately at the same positions, where also the

Table 3. Analysis of the anisometry and ratio of patchy part to particle volume derived through the CMXRF measurements. For the evaluation of the anisometry, length, width, and height of the particles were established using the full 3D maps and the ratios length/width, length/height, width/height displayed for comparison. The ratio of the length/width measured with optical microscopy is also shown for comparison.

Composition	Type	Anisometry from Optical Microscopy	Anisometry from CMXRF (+/- 0.1)	Percentage of patchy part to complete volume [%]
NaCl + PS	S1	1.14	1.1, 1.1, 1	9
NaCl + PS + Heat	S1*	1.05	1, 1.3, 1.3	9
Na_2SiO_3 without magnet	S2*	1.31	1.3, 1.9, 1.4	–
Na_2SiO_3	S2	1.29	1.3, 1.9, 1.5	8
Na_2SiO_3 + MFC	S4	1.48	1.5, 2, 1.4	17

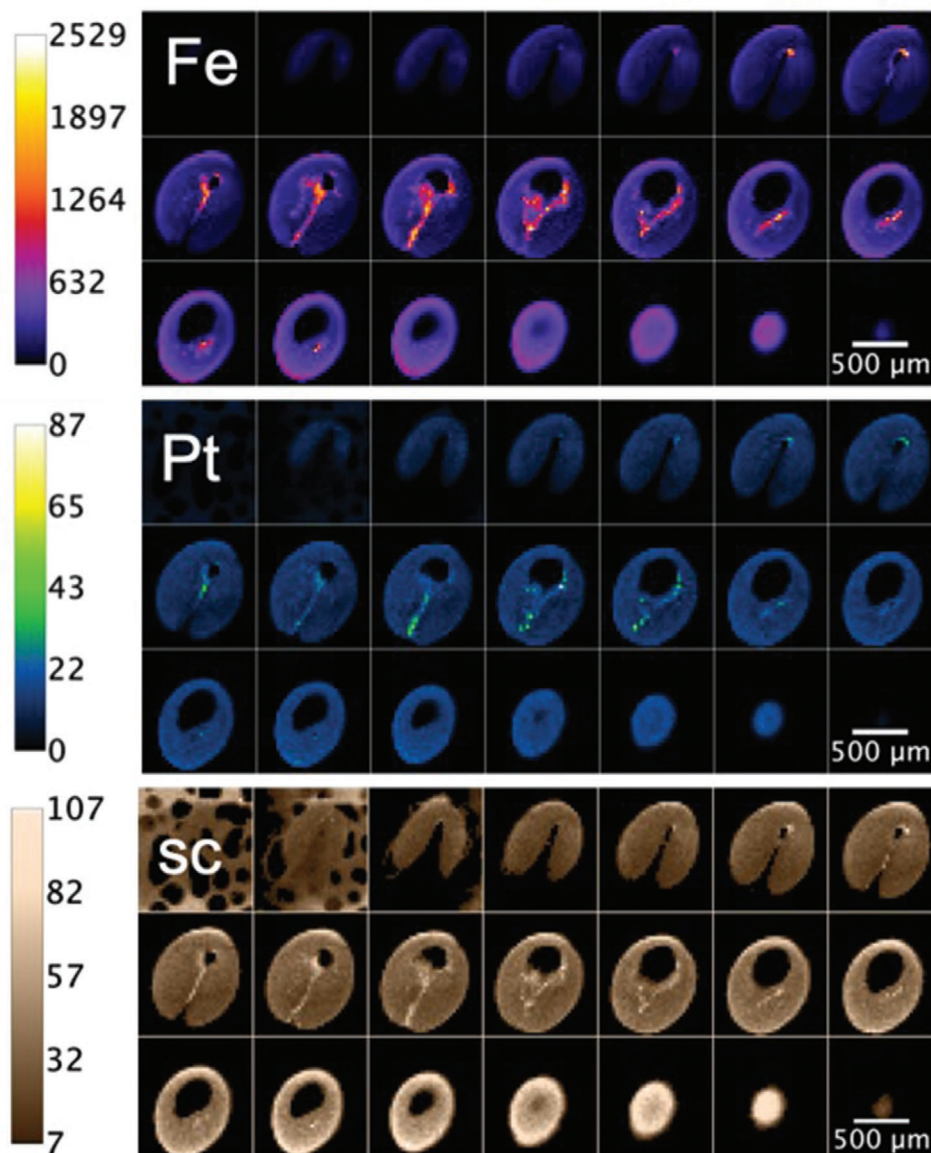


Figure 10. Distribution of Fe (top) and Pt (middle) inside a particle of type S2 (Na_2SiO_3) obtained in the absence of a magnetic field (S2^*). The bottom images show the distribution of the density of the particle through the analysis of scattered radiation. The color scales show the measured intensity of the fluorescence signal in counts per second (CPS).

density of the particle is enhanced. This generally holds true for all analyzed particles with slight variations (see the set of virtual slices in the Supporting Information for details). In absence of an applied magnetic field during the forming process, the Fe/Pt distribution does not form a patch on the surface of the supraparticles but accumulates in their centers presumably on top of the fold formed by the crescent-shaped bottom.

Similar experiments were conducted on twelve supraparticles from all suitable types (S1, S2, S4, see Figure 2) and one representative result is shown for each type in Figure 11. For all measurements, a virtual slice through approximately the middle of the particles was chosen for comparison, see the exact position of the selected slides in Figures S3–S7, Supporting Information. From left to the right the Fe and Pt distributions and the scattering are shown. All images are scaled to

the highest contrast with the individual intensity scales facilitating a comparison between the different classes.

The results are in correspondence with all other evidence. Without a magnet, the catalyst is distributed rather evenly in the particle, with conglomerates that are not necessarily on its surface, as seen by the stripe-like structure in the middle of the particle. With a magnet and a sodium silicate matrix (type S2 particle), the patch is localized in a small volume determined by the position of the magnet during preparation. When MFC and Na_2SiO_3 were added (type S4 particle), Fe/Pt is distributed more heterogeneously over larger volumes, because the movement to the magnet apparently is impeded due to the network characteristics of MFC. For this S4 type, no well-defined patchy part is formed, which will change the propulsion properties of the particles. With PS included in the matrix (type S1 particles),

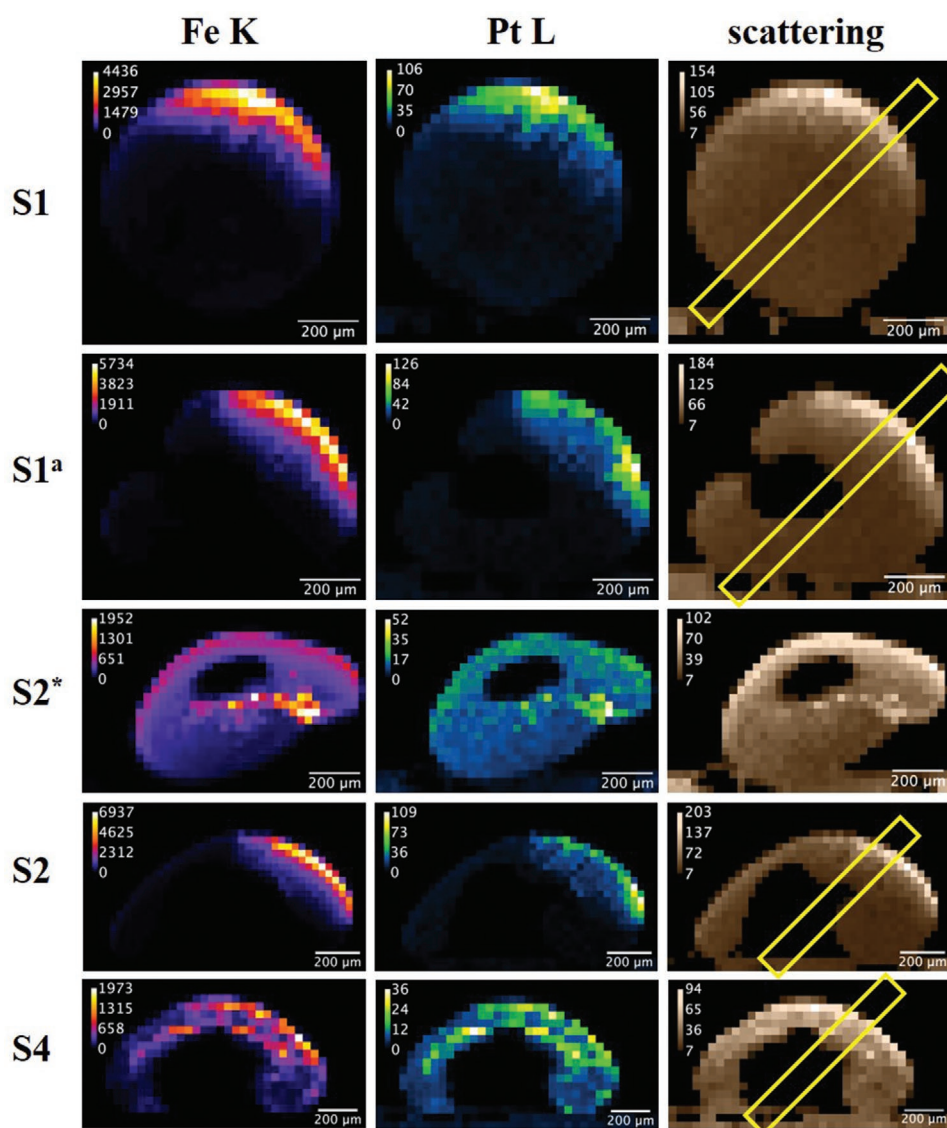


Figure 11. Comparison of the typical shape and patch localization (via the localization of the different metals) for different types of supraparticles obtained in the presence of a directing magnetic field (except the third row). The color scales show the measured intensity of the fluorescence signal in CPS.

a well-defined patchy part is visible irrespective of heating. That means no further migration of Fe/Pt occurs due to heating, which confirms that this approach is a very good one for subsequent modification of the supraparticles.

For all particles prepared with magnetic field force, the patchy part is preferentially located towards the surface but also up to more than 200 μm into the inside. This is illustrated in **Figure 12** where the intensities are plotted over the relative distance from the surface (position 0 μm) along the marked paths in **Figure 11**, see Supporting Information for details. By evaluating the scattering and fluorescence profiles, different regions can be identified qualitatively. There are regions where the probing volume is inside the particle (marked with grey boxes), regions without material and regions where the volume enters the carbon tape that carries the sample (marked with yellow boxes), see also **Figure 12** for comparison. For particles with Na_2SiO_3 (S2) and with PS (S1), the distribution of

Fe/Pt is highest at the surface and decreases into the particle. This decrease is due to absorption inside the particle as well as the distribution of the elements. There are two aspects to be considered. First, the attenuation is pronouncedly different from element to element due to the energy dependency of the linear mass absorption coefficient.^[53] Therefore, the Pt signal is less attenuated than the Fe signal, resulting in a smaller decreasing trend of the Pt signal compared to the Fe signal. Second, the Pt signal is overall less intense than the Fe signal (see the intensity scales in **Figure 12**) and cannot be completely separated in some points from the scattered signal. These two effects lead to a detected Pt signal at depths, where the iron signal is already very low compared to the signal at the surface and an apparent signal of Pt inside the carbon tape. Nevertheless, a qualitative analysis of the element profiles is feasible. Thus, specifically in the case of the profiles of the particle with MFC and Na_2SiO_3 (S4), a heterogeneous distribution is

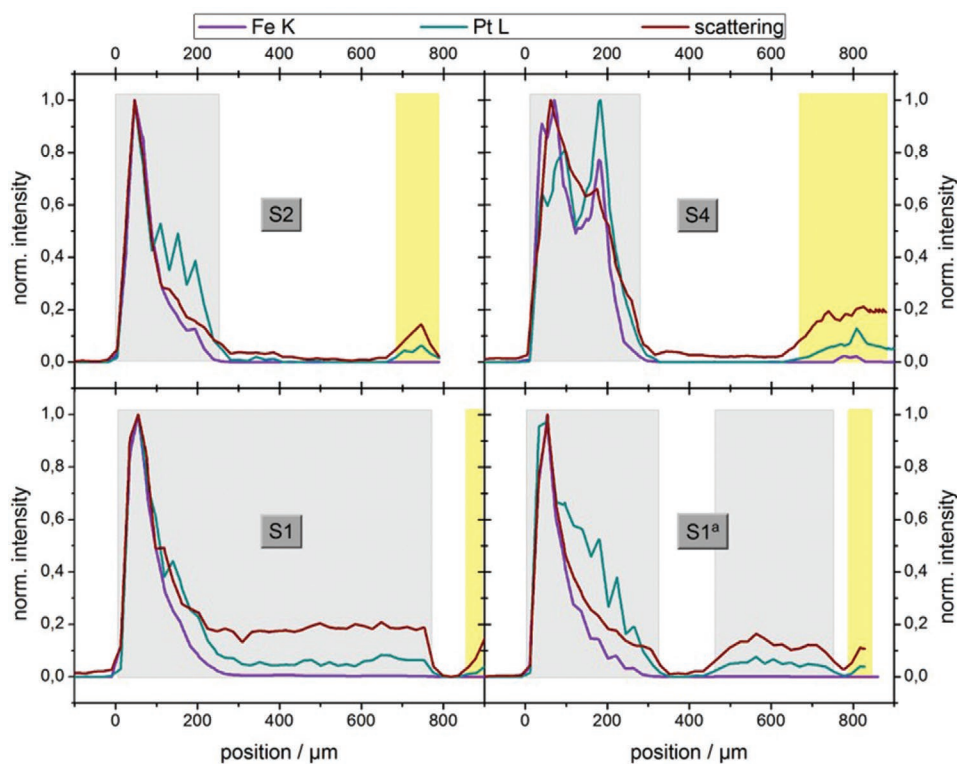


Figure 12. Line profiles along the marked paths of Figure 11. The intensities are plotted as a function of position with the surface at 0 μm . The decrease to higher position values is a combination of absorption effects and localization. Through the evaluation of the scattering and fluorescence profiles, different regions can be identified qualitatively. The probing volume is either inside the particle (grey box), in areas without material, or inside the carbon tape which is used as sample support (yellow box), see also Figure 11 for comparison.

identified. Here the $\text{Fe}_3\text{O}_4@Pt$ nanoparticles are found much deeper within the supraparticles and only for the particles with MFC and Na_2SiO_3 (type S4) no connected homogeneous patchy part is formed, possibly changing the movement characteristics of the corresponding particle type.

Table 3 lists the anisometry of the supraparticles of Figure 11 calculated using the CMXRF measurements. For defining the shape of the particles, a threshold of 7 cps of the scattering signal was defined and then a coordinate system was used to extract values for the height, width, and length of the supraparticles. The three anisometry values in Table 3 represent the ratio of length/width, length/height, width/height. Particles made of Na_2SiO_3 with and without adding MFC have an elliptical shape with similar dimensions in one class. The values of anisometry for the particles made of NaCl and PS show either a more spherical shape (values closer to 1) as presented in the selected measurements or a completely asymmetric shape (not shown here).

To have a rough qualitative comparison, the ratio of the patchy part in relation to the full volume was calculated using the number of pixels which were defined as containing $\text{Fe}_3\text{O}_4@Pt$ nanoparticles divided by the overall pixel amount of the particles. The threshold for the patchy part was defined as the intensity value where the maximum signal of the sum of the Fe K and Pt L intensity is decreased to 20%. This procedure does not yield quantitative values of the amount of $\text{Fe}_3\text{O}_4@Pt$ nanoparticles in the supraparticles and therefore cannot be compared to the quantities given in Table 2. However, the procedure can be

used to identify the number of pixels over which the $\text{Fe}_3\text{O}_4@Pt$ particles are distributed through the supraparticles. Thus, the ratio of the patchy part pixels to the total particle pixels serves as a measure of the distribution of the patchy part. As expected, the ratio of the patchy part pixels to the particle pixels is much smaller for the particles made with Na_2SiO_3 or PS (8–9%) compared to the particles made with MFC and Na_2SiO_3 (17%), as apparently, the MFC hinders the free movement of the magnetic catalyst nanoparticles.

4.4. Comparison of the Different Particle Types with Respect to Mechanical Stability and the Capacity for Self-Propulsion

The central part of this work was to produce supraparticles that can self-propel in H_2O_2 solution but can do so without disintegrating during that process. Of course, if the H_2O_2 decomposition is suppressed the particles will remain stable in that solution, but then also propulsion is impossible. Accordingly, the ideal particle is one with full catalytic activity, that can sustain all mechanical forces that may arise from the oxygen formation in pores of the supraparticles.

Data relating the different types of modifications to the mechanical stability are shown in Figure 13 and summarized in Table 4 together with the ability of the supraparticles to self-propel in the H_2O_2 solution. Figure 13 shows the results of the particles' disintegration rate as a function of time after placing them in a 5% H_2O_2 solution. As described earlier, the FS

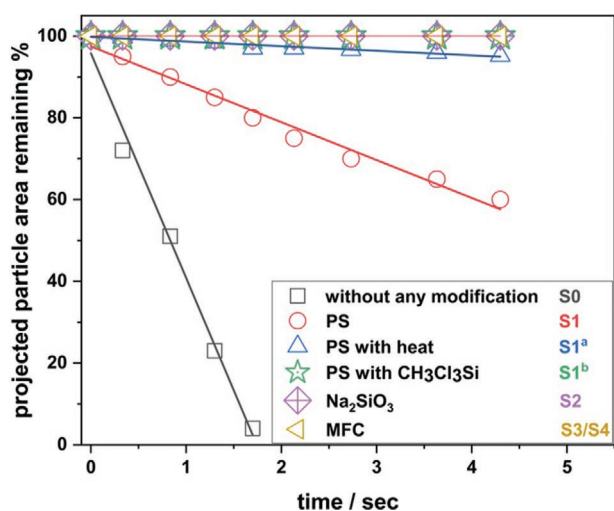


Figure 13. Disintegration rate of supraparticles treated differently to provide mechanical strength and hydrophobicity. Rapid disintegration is observed for the particles without any treatment, slow disintegration is observed for heat-treated particles with PS, and last no disintegration at all is observed for the particles treated with CH₃Cl₃Si and Na₂SiO₃ (with and without MFC).

particles without any treatment, S0, disintegrate completely as soon as they are immersed in H₂O₂ solution. S1 type particles including PS, also start disintegrating as soon as they are put on H₂O₂ solution and lose about 50% within 4–5 s. The particles kept in the oven for about 8 h at 115 °C (4.2.2, S1^a), thereby being well above the glass transition temperature of the PS and forming a composite material of PS and FS, are much more stable compared to the ones without any treatment, but still disintegrate to some extent. In contrast, the particles treated with CH₃Cl₃Si (S1^b; see Section 4.2.3) are long-time stable. However, due to over-hydrophobization, the CH₃Cl₃Si modified particles did not show any motion when immersed in H₂O₂ solution, as apparently the catalytic Fe₃O₄@Pt nanoparticles are no longer accessible. Na₂SiO₃(S2), MFC(S3), and Na₂SO₃&MFC (S4) modified particles did not show any disintegration during self-propulsion experiments; however, the separation between the patch and the rest of the particle in these particles was not found to be as sharp as observed in S1 type particles due to ingredients' blocking the diffusion of the catalyst while drying of the particles. Especially S3 type particles show a very random distribution of the catalyst (see Figure 7); therefore, this class was not considered as suitable propellers for further studies.

Table 4. Comparison of mechanical stability in H₂O₂ solution and the ability for self-propelled motion in this solution for the different types of particles (+++: very good; +: poor; -: no motion was observed).

Method		Stability	Self-Propulsion
PS	S1	+ / ++	+ / ++
Heat	S1 ^a	+ / +++	+ / +++
CH ₃ Cl ₃ Si	S1 ^b	+++	-
Na ₂ SiO ₃	S2	+++	+ / +++
MFC	S3	+++	+ / ++
Na ₂ SiO ₃ +MFC	S4	+++	+++

The joint usage of Na₂SiO₃ and MFC (at lower concentrations than in S3 particles) seems to be the best method to fabricate long-term stable particles that retain the catalytic activity required for self-propulsion. PS addition with heat treatment is another convenient method, which leads to robust particles with good catalytic activity. In both cases, one adds a polymeric compound to the more brittle FS particles, which should impart some elastic properties to the supraparticles and thereby enhance substantially their toughness during self-propulsion. Interestingly, here the MFC/Na₂SiO₃ (S4) addition still performs clearly better than the PS containing heat-treated S1^a particles (Figure 13). Apparently, the MFC network formed within the supraparticles gives particular strength here and therefore is the best choice for forming mechanically stable supraparticles with good capacity for self-propulsion (see Table 4).

5. Conclusions

We report the formation and characterization of anisometric self-assembled patchy particles that could move by self-propulsion. The particles were based on FS and prepared by the previously described method^[36] of evaporation of mm-sized droplets on a bent superhydrophobic surface. Patchy particles were obtained by directing catalytically active Fe₃O₄@Pt nanoparticles (that decompose H₂O₂ and thereby drive self-propulsion) with a magnet to the desired position. However, the main challenge encountered in the making of these supraparticles is their fragility during self-propulsion driven by H₂O₂ decomposition that leads to oxygen formation within the pores of the supraparticles. The resulting pressure then leads rapidly to substantial disintegration of the mechanically to instable pure FS supraparticles. Accordingly, our aim was to enhance their stability by means of additives that may lower the hydrophilicity of the supraparticles and enhance their mechanical stability, for instance by adding elastic properties to the otherwise rather brittle FS particles. The other central aim was to gather detailed knowledge about the structure of the catalytically active patch, as its size and location are of central importance for the self-propulsion motion of such particles.

Employing CH₃Cl₃Si by CVD as a hydrophobization agent led to long-time stable particles. However, even for the application of very small amounts of CH₃Cl₃Si, and very short application times of 3–5 s, the particles became inactivated and did no longer show any motion during self-propulsion experiments. Heating was another approach to hydrophobize the particles as it reduces the number of Si-OH groups. However, this method also led to the deactivation of the catalytic activity and no self-propulsion was observed.

In the next research step, PS nanoparticles were used for hydrophobization and in addition, lower the density of the particles and thereby improve the swimming properties. Just the addition of PS microparticles in the assemblies does not improve their stability, but after a heat treatment well above the glass transition temperature of PS homogenous supraparticles of enhanced mechanical stability are obtained due to the formation of a hybrid material, which are stable for long times in H₂O₂ solution and able to self-propel.

Another approach that leads to the formation of stable particles is the addition of Na₂SiO₃. Interestingly it is not only mechanically stabilizing the supraparticles, but at the same time allows to control the anisometry, thereby eliminating the need to apply NaCl for this purpose (NaCl adds to the fragility of the supraparticles by dissolving in aqueous solution). Finally, we also employed a naturally derived material, MFC as an additive to control the particles' properties and confer additional functionality. By creating a highly porous network structure, MFC adds a significant contribution to the stability of the particles by aligning internally and structurally reinforcing the material. However, due to the properties of the MFC, it is difficult to obtain assemblies with well-defined catalytic patches. This problem could be circumvented by using MFC and Na₂SiO₃ together and lowering the MFC content. In this fashion, one obtains particles with regular shape, which are very well suited for self-propulsion.

The structural quality of the particles and especially, their internal structure, including the distribution of the catalytically active Fe₃O₄@Pt nanoparticles, was imaged by means of CMXRF. These results show nicely that the Fe₃O₄@Pt nanoparticles are embedded rather deeply in the supraparticles, but nonetheless show a well-defined structure, where too high amounts of MFC hinder the free motion of the Fe₃O₄@Pt nanoparticles, thereby leading to larger patch sizes.

To conclude, the aim of this study was to prepare patchy particles to be used for self-propulsion purposes. The biggest obstacle was the fact that such porous particles can disintegrate due to the pressure build-up during oxygen formation in H₂O₂ decomposition, thereby largely limiting their lifetime in a propulsion experiment. By varying the components of the supraparticles, we managed to obtain stable patchy particles, with the MFC&Na₂SiO₃ modified particles being the most promising ones. The stability of the patchy mechanically reinforced supraparticles was proven by preliminary self-propulsion experiments.

Supporting Information

Supporting Information is available from the Wiley Online Library or from the author.

Acknowledgements

Financial support of this project by the DAAD (GSSP program) and the DFG, (via IRTG 1524 SSN1) at TUB is gratefully acknowledged. Furthermore, US NSF grant CBET-1604116 is acknowledged for additional financial support. For help with the SEM images the authors thank MSc Chunning Sun and Christoph Fahrenson (both TUB) and Chuck Mooney (NCSU). For the TEM images we are grateful to Jan Simke and Selve Sören (TUB).

Open access funding enabled and organized by Projekt DEAL.

Conflict of Interest

The authors declare no conflict of interest.

Data Availability Statement

Research data are not shared.

Keywords

anisometric, fumed silica, magnetite, microfibrillated cellulose, platinum catalyst, superhydrophobic

Received: December 15, 2020

Revised: February 27, 2021

Published online:

- [1] Y. Xia, T. D. Nguyen, M. Yang, B. Lee, A. Santos, P. Podsiadlo, Z. Tang, S. C. Glotzer, N. A. Kotov, *Nat. Nanotechnol.* **2012**, *7*, 479.
- [2] O. D. Velev, S. Gupta, *Adv. Mater.* **2009**, *21*, 1897.
- [3] X. Feng, L. Jiang, *Adv. Mater.* **2006**, *18*, 3063.
- [4] F. Li, D. P. Josephson, A. Stein, *Angew. Chem., Int. Ed.* **2011**, *50*, 360.
- [5] H. Goesmann, C. Feldmann, *Angew. Chem., Int. Ed.* **2010**, *49*, 1362.
- [6] J. F. Galisteo-López, M. Ibsate, R. Sapienza, L. S. Froufe-Pérez, Ú. Blanco, C. López, *Adv. Mater.* **2011**, *23*, 30.
- [7] D. R. Rolison, *Science* **2003**, *299*, 1698.
- [8] A. Cho, *Science* **2003**, *299*, 1684.
- [9] Z. Lu, Y. Yin, H. Kim, S. Kwon, H. Lee, J. Ge, J. Goebel, L. He, J. Kim, *J. Am. Chem. Soc.* **2009**, *131*, 15687.
- [10] J. Kim, Y. Song, L. He, H. Kim, H. Lee, W. Park, Y. Yin, S. Kwon, *Small* **2011**, *7*, 1163.
- [11] D. A. Weitz, T. Kanai, D. Lee, H. C. Shum, R. K. Shah, *Adv. Mater.* **2010**, *22*, 4998.
- [12] N. Vogel, C. K. Weiss, K. Landfester, *Soft Matter* **2012**, *8*, 4044.
- [13] L. Isa, K. Kumar, M. Müller, J. Grolig, M. Textor, E. Reimhult, *ACS Nano* **2010**, *4*, 5665.
- [14] Z. Xiao, A. Wang, J. Perumal, D. P. Kim, *Adv. Funct. Mater.* **2010**, *20*, 1473.
- [15] V. Rastogi, K. P. Velikov, O. D. Velev, *Phys. Chem. Chem. Phys.* **2010**, *12*, 11975.
- [16] S. N. Yin, C. F. Wang, Z. Y. Yu, J. Wang, S. S. Liu, S. Chen, *Adv. Mater.* **2011**, *23*, 2915.
- [17] S.-M. Yang, D. J. Pine, G.-R. Yi, J. H. Moon, S. B. Park, *Adv. Mater.* **2004**, *16*, 605.
- [18] Z. Shen, Y. Zhu, L. Wu, B. You, J. Zi, *Langmuir* **2010**, *26*, 6604.
- [19] Z. Yu, L. Chen, S. Chen, *J. Mater. Chem.* **2010**, *20*, 6182.
- [20] U. Jonas, W. Knoll, K. Burkert, J. Wang, H. Ottleben, T. Neumann, *Langmuir* **2007**, *23*, 3478.
- [21] V. Rastogi, O. D. Velev, *Biomicrofluidics* **2007**, *1*, 014107.
- [22] J. T. Wang, J. Wang, J. J. Han, *Small* **2011**, *7*, 1728.
- [23] Z. Yu, C. F. Wang, L. Ling, L. Chen, S. Chen, *Angew. Chem., Int. Ed.* **2012**, *51*, 2375.
- [24] Y. S. Cho, S. H. Kim, G. R. Yi, S. M. Yang, *Colloids Surf., A* **2009**, *345*, 237.
- [25] Y.-S. Cho, G.-R. Yi, S.-H. Kim, M. T. Elsesser, D. R. Breed, S.-M. Yang, *J. Colloid Interface Sci.* **2008**, *318*, 124.
- [26] D.-W. Lee, M.-H. Jin, C.-B. Lee, D. Oh, S.-K. Ryi, J.-S. Park, J.-S. Bae, Y.-J. Lee, S.-J. Park, Y.-C. Choi, *Nanoscale* **2014**, *6*, 3483.
- [27] V. Rastogi, S. Melle, O. G. Calderón, A. A. García, M. Marquez, O. D. Velev, *Adv. Mater.* **2008**, *20*, 4263.
- [28] V. Rastogi, A. A. Garcia, M. Marquez, O. D. Velev, *Macromol. Rapid Commun.* **2010**, *31*, 190.
- [29] M. Sperling, O. D. Velev, M. Gradziński, *Angew. Chem., Int. Ed.* **2014**, *53*, 586.
- [30] O. D. Velev, *Science* **2000**, *287*, 2240.
- [31] R. D. Deegan, O. Bakajin, T. F. Dupont, G. Huber, S. R. Nagel, T. A. Witten, *Nature* **1997**, *389*, 827.
- [32] T. Still, P. J. Yunker, A. G. Yodh, *Langmuir* **2012**, *28*, 4984.
- [33] S. Zellmer, G. Garnweitner, T. Breinlinger, T. Kraft, C. Schilde, *ACS Nano* **2015**, *9*, 10749.
- [34] W. Liu, M. Kappl, H. J. Butt, *ACS Nano* **2019**, *13*, 13949.

- [35] S. Wooh, H. Huesmann, M. N. Tahir, M. Paven, K. Wichmann, D. Vollmer, W. Tremel, P. Papadopoulos, H.-J. Butt, *Adv. Mater.* **2015**, *27*, 7338.
- [36] M. Sperling, V. J. Spiering, O. D. Velev, M. Gradzielski, *Part. Part. Syst. Charact.* **2017**, *34*, 1600176.
- [37] B. D. Mattos, B. L. Tardy, L. G. Greca, T. Kämäräinen, W. Xiang, O. Cusola, W. L. E. Magalhães, O. J. Rojas, *Sci. Adv.* **2020**, *6*, eaaz7328.
- [38] T. Lindström, A. Dorris, S. Moritz, D. Klemm, D. Gray, F. Kramer, M. Ankerfors, *Angew. Chem., Int. Ed.* **2011**, *50*, 5438.
- [39] N. Lavoine, I. Desloges, A. Dufresne, J. Bras, *Carbohydr. Polym.* **2012**, *90*, 735.
- [40] Y. S. Kang, S. Risbud, J. F. Rabolt, P. Stroeve, *Chem. Mater.* **1996**, *8*, 2209.
- [41] E. Z. Basta, *Mineral. Mag. J. Mineral. Soc.* **1957**, *31*, 431.
- [42] H. E. Swanson, E. Tatge, in *Natl. Bur. Stand. (U.S.), Circ. 539*, Washington, DC **1953**, p. 31.
- [43] "www.hkcm.de", can be found under <https://www.hkcm.de/desk.php/?l=en&fav=6187lid> (accessed: March 2019).
- [44] R. Kushwaha, *Int. J. Comput. Graph. Animat.* **2015**, *5*, 15.
- [45] L. Li, J. Wang, T. Li, W. Song, G. Zhang, *Soft Matter* **2014**, *10*, 7511.
- [46] C. A. Schneider, W. S. Rasband, K. W. Eliceiri, *Nat. Methods* **2012**, *9*, 671.
- [47] C. Seim, C. Laurenze-Landsberg, B. Schröder-Smeibidl, I. Mantouvalou, C. de Boer, B. Kanngießer, *J. Anal. At. Spectrom.* **2014**, *29*, 1354.
- [48] F. Czerwinski, *Heat Treatment – Conventional and Novel Applications*, InTech, Rijeka **2012**.
- [49] L. Zaretskiy, *Int. J. Met.* **2019**, *13*, 58.
- [50] C. Conti, A. Botteon, C. Colombo, M. Realini, P. Matousek, P. Vandenabeele, B. Laforce, B. Vekemans, L. Vincze, *Anal. Methods* **2018**, *10*, 3837.
- [51] K. G. McIntosh, N. L. Cordes, B. M. Patterson, G. J. Havrilla, *J. Anal. At. Spectrom.* **2015**, *30*, 1511.
- [52] T. Lachmann, G. Van Der Snickt, M. Haschke, I. Mantouvalou, *J. Anal. At. Spectrom.* **2016**, *31*, 1989.
- [53] I. Mantouvalou, T. Lachmann, S. P. Singh, K. Vogel-Mikuš, B. Kanngießer, *Anal. Chem.* **2017**, *89*, 5453.